2018 25th International Lightning Detection Conference &
7th International Lightning Meteorology Conference
March 12 - 15 | Ft. Lauderdale, Florida, USA

Spatial characteristics of lightning relative to supercell kinematics and microphysics

Sarah M. Stough, Lawrence D. Carey
Department of Atmospheric Science
University of Alabama in Huntsville
Huntsville, Alabama, United States
sarah.stough@nsstc.uah.edu

Christopher J. Schultz, Daniel J. Cecil
Earth Science Office
NASA Marshall Space Flight Center
Huntsville, Alabama, United States

***Abstract*— Rapid increases in total lightning flash rate, termed lightning jumps, are often observed prior to high-impact convective phenomena. Relationships between lightning jumps and substantial increases in quantifiable bulk updraft properties have been shown. However, the details that support these relationships are not well resolved, particularly with respect to variability of flash rate trends in response to kinematic properties and specific, process-based connections with high-impact phenomena. This study addresses detail within the complex relationships between lightning, kinematics, and microphysics via observations of a supercell thunderstorm. Correspondence between flash rates and bulk updraft characteristics agreed with established relationships while flash properties varied between significant changes in flash rate. Dominant flash size and altitudes of flash initiation during lightning jumps corresponded spatially with a complex combination of updraft characteristics and graupel distribution. Flashes associated with a rapid decrease in flash rate showed a weaker spatial relationship with the updraft.**

Keywords—supercell; Doppler radar; thunderstorm microphysics

I. INTRODUCTION

Observations relating rapid increases in total lightning flash rate to high-impact phenomena have been frequently reported in the literature, motivating the study of lightning as a metric of thunderstorm intensity [e.g., Williams et al. 1999; Goodman et al. 2005; Schultz et al. 2009, 2011, 2015, 2017; Darden et al. 2010; Gatlin and Goodman 2010]. Flash rates have generally been shown to relate to properties such as thunderstorm graupel mass or graupel volume, updraft velocity, and measures of updraft size, such as the volume of the updraft in which vertical velocities are greater than or equal to $10\ \mathrm{m\ s^{-1}}$ [e.g., Carey and Rutledge 1996, 2000; Lang and Rutledge 2002; Deierling et al. 2008; Deierling and Petersen 2008; Calhoun et al. 2013, 2014]. Meanwhile, quantified rapid increases in flash rate, referred to as lightning jumps, have been shown to be related to more significant changes in the updraft of a thunderstorm [Schultz et al. 2015, 2017]. In particular, quantified lightning jumps correspond with changes in the $10\ \mathrm{m\ s^{-1}}$ updraft volume and maximum updraft speeds that are roughly four and five times greater, respectively, than those that occur in association with non-jump increases in flash rate [Schultz et al. 2017].

Relationships between flash rates and updraft properties have physical roots in the suggested role of the updraft in the non-inductive charging mechanism, storm-scale charge separation, and subsequent flash production [Reynolds et al. 1957; Takahashi 1978; Carey and Rutledge 1996, 2000; Deierling and Petersen 2008]. However, complexities within the physical underpinnings of these relationships have not been well resolved. For instance, the relative roles of kinematics and microphysics in the generation of a lightning jump, connections between lightning and specific thunderstorm processes contributing to severe

This work was supported by National Aeronautics and Space Administration (NASA) Severe Storms Research funding (NNH14ZDA001N), provided to University of Alabama in Huntsville authors under contract from the NASA Marshall Space Flight Center (NNM11AA01A)

weather, and the mechanisms behind rapid decreases in flash rate, including those occasionally observed prior to tornadogenesis, are not well understood. In particular, lightning's connection with and response to vertical kinematics have not been deeply explored with respect to downdraft-generated phenomena. Investigation of these complex, interconnected properties and processes related to high-impact phenomena requires more detailed analyses at finer spatial scales than reported in many studies of bulk thunderstorm properties.

The most productive path to understanding details that connect lightning and thunderstorm processes ultimately requires a combination of well-observed thunderstorm events and high-resolution analysis of process afforded by numerical simulations. This study serves as an introductory analysis of a well-observed thunderstorm case in which the details of flash properties, microphysics, and kinematics are considered during significant trends in lightning flash rates. Information from available radar and lightning data is discussed, where results include detailed descriptions of lightning, microphysics, and kinematic behaviors; their variation in space and time; and possible connections that may be evaluated through additional observations and future implementation of a modeling component.

II. DATA AND METHODS

A. *01 April 2016 Supercell Case*

A supercell that occurred on 01 April 2016 in northern Alabama serves as the thunderstorm of interest for this study. It was observed by a suite of instrumentation during a Verification of the Origins of Rotation in Tornadoes Experiment – Southeast (VORTEX-SE) intensive operations period, including multiple Doppler radars and the North Alabama Lightning Mapping Array (NALMA). Instrumentation platforms within the sampling domain relevant to this study are shown in Fig. 1. While data were collected within the sampling domain for several hours prior to, during, and following passage of the supercell, the analysis period of the storm is limited to the 0100 UTC to 0200 UTC during which time two nearby radars were providing observations. The supercell produced an EF2 tornado that was reported between 0157 UTC and 0212 UTC. No other reports of severe weather were documented during the analysis period.

In addition to providing a well-sampled case, the supercell mode represented by this storm presents the opportunity to evaluate properties of interest within quasi-steady storm structure. Additionally, the supercell storm mode includes prevalent kinematic regions for evaluation alongside well-developed microphysical fields and lightning properties. The main updraft, forward flank downdraft (FFD), and rear flank downdraft (RFD) are the primary vertical kinematic regions identified in supercell structure. While the RFD is thought to initially result from storm flow and pressure pertubations, both the RFD and FFD are supported by a combination of precipitation loading and latent heat exchange as a result of microphysical processes [Hookings 1965; Lemon and Doswell 1979; Srivastava et al. 1985, 1987; Knupp 1987, 1988; Vonnegut 1996; Tong et al. 1998; Naylor et al. 2012].

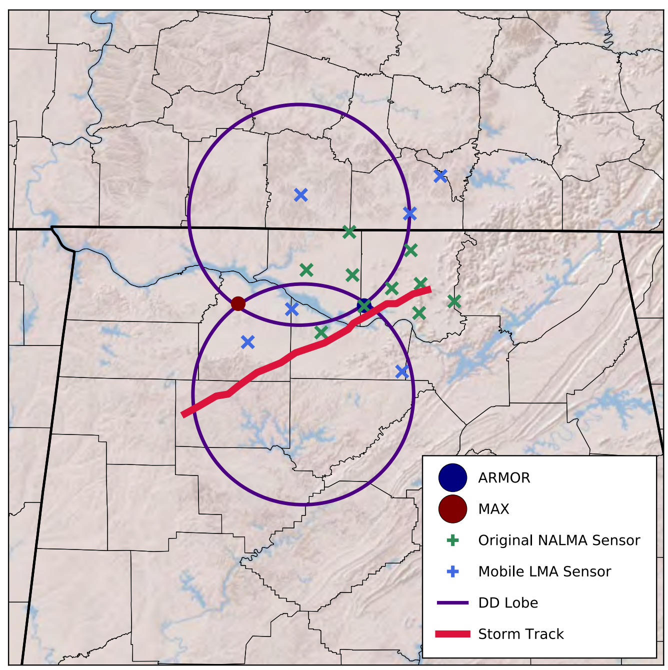

Fig. 1: VORTEX-SE sampling domain and relevant instrumentation. The ARMOR and MAX radar are plotted as blue and red dots, respectively, while the dual-Doppler lobes determined from 30° beam crossing are marked by the purple circles. The 10 LMA sensors that usually comprise the NALMA within northern Alabama and southern Tennessee are plotted as green crosses and the mobile LMA sensors added to the network for the VORTEX-SE project are plotted as blue crosses. The path of the storm of interest is plotted as a red line, where this analysis focuses upon the period during which the storm propagated through the southern dual-Doppler lobe.

B. *Lightning Data and Processing Methods*

The NALMA typically consists of a configuration of twelve sensors located in northern Alabama, southern Tennessee, and northwestern Georgia that detect very high frequency (VHF) emissions during the propagation of lightning channels [Rison et al. 1999]. However, six mobile LMA sensors were added to the standard NALMA domain during the VORTEX-SE field project, providing additional network sensitivity. A total of 16 of the 18 available sensors were active during the analysis period of this supercell, all located within northern Alabama and southern Tennessee [NASA 2001]. VHF sources detected by LMA sensors are located in time and space utilizing a time of arrival technique [Thomas et al. 2004]. While data from a minimum of four sensors are required to resolve the time and location of a source, six or more sensors are typically utilized in practice to reduce the inclusion of noise. Source data are subject to location errors on the order of 1 km in the vertical and 500 m in the horizontal within 100 km of the LMA network center, outside of which they may grow to surpass convective scales [Koshak et al. 2004; McCaul et al. 2005]. The storm of interest for this study remained within 100 km of the NALMA center for the duration of its analysis.

NALMA source data were clustered into flashes with the python-based open-source “lmatools” software [Bruning 2013], in which a set of spatial and temporal criteria are employed to group sources into flashes according to the DBSCAN technique [Bruning 2013; Fuchs et al. 2015, 2016]. For this study, a spatial threshold of 1 km and a temporal threshold of 0.3 s were used to identify sources within a flash, consistent with the McCaul et al. [2009] methods historically utilized with NALMA data [e.g., McCaul et al. 2009; Schultz et al. 2009, 2011]. A maximum flash duration of 3 s was also imposed. Sources were additionally required to have been detected by a minimum of six sensors in order to be considered for flash clustering.

As part of flash clustering, the lmatools software is also capable of providing a number of flash properties, including the time and three-dimensional locations of flash initiation, the number of sources within each flash, flash area and volume. Lmatools optionally provides post-processed gridded products of flash-clustered data. Flash initiation density (FID), or the number of lightning flashes that occur within a given grid pixel, and flash extent density (FED), or the number of lightning branches ot pass through a given grid pixel, were gridded with 1.0 km horizontal and 0.5 km vertical grid spacing. For gridded products and subsequent flash-based analyses, only flashes with a minimum of 10 sources were considered to reduce the likelihood of including noise erroneously identified as flashes.

Processed lightning flash data were associated with the supercell according to the methods described in Stough et al. [2017]. Briefly, using the Warning Decision Support System – Integrated Information (WDSS-II) software, storm objects were identified using environmental and radar reflectivity data [Lakshmanan et al. 2007]. Storm boundaries based on these objects were used to isolate lightning flashes associated with the storm of interest. Flashes collected via storm tracking were binned in 2-min intervals and processed to determine 1-min flash rate and the presence of any lightning jumps and lightning dives, or rapid decreases in flash rate, according to the Schultz et al. [2009, 2015] 2σ lightning jump algorithm (LJA). A lightning jump (dive) is determined for a 2-min interval during which the change in flash rate is greater (less) than at least two standard deviations of the change in flash rate observed over the prior 10-min period. Additionally, the minimum flash rate must be at least 10.0 flashes per minute (fpm) and a jump cannot follow another by fewer than 6 min. In the case of a lightning dive, the flash rate must have been at least 10.0 fpm within 4 minutes prior to the dive. Note that lightning dive flash rate requirements are not implemented in the traditional Schultz et al. [2009, 2015] 2σ LJA. The “σ-level” associated with the jump (dive) is the number of standard deviations by which the increase in flash rate at the time of the jump exceeded (fell below) the recent history of change in flash rate. In the case of a lightning jump, the σ-level reflects the intensity of the jump, and by extension, the change in intensity of the updraft as inferred through a property such as maximum speed or 10 m s^{-1} volume [Schultz et al. 2017].

C. *Radar Data and Processing Methods*

The supercell of interest was best sampled by the fixed-site C-band Advanced Radar for Meteorological and Operational Research

(ARMOR; Schultz et al. 2012; Knupp et al. 2014), though was also within adequate range of the Mobile Alabama X-band radar to allow dual-Doppler analysis for vertical wind retrievals. Data collected from the ARMOR are primarily discussed herein, while Doppler velocity data collected from the MAX radar were also utilized.

Prior to conducting kinematic analysis, the ARMOR and MAX velocity data were manually edited and dealiased using the National Center of Atmospheric Research (NCAR) SOLOIII software [Oye et al. 1995; Vacek 2017]. These data were then gridded to a common Cartesian coordinate system with a 1 km horizontal and 0.5 km vertical grid spacing using the NCAR Radx software [Heistermann et al. 2014; Vacek 2017]. Dual-Doppler analysis was then performed using the NCAR Custom Editing and Display of Reduced Information in Cartesian space (CEDRIC) software for the retrieval of vertical velocity data [Mohr et al. 1986; Miller and Frederick 1998; Vacek 2017].

Microphysical analysis was accomplished through use of hydrometeor identification (HID) via the Dolan et al. [2013] HID algorithm with ARMOR data. The HID algorithm identifies the dominant precipitation-sized hydrometeor type in a radar gate or grid pixel based on weighted polarimetric radar data and temperature data inputs that are evaluated using a fuzzy logic scheme. There are ten possible hydrometeor types, including melting hail/large raindrops, hail, high-density graupel, low-density graupel, aggregates, vertical ice, ice crystals, wet snow, drizzle, and rain. The polarimetric data considered include differential reflectivity (Z_{DR}), specific differential phase (K_{DP}), and copolar cross correlation coefficient (ρ_{HV}) in addition to the horizontal reflectivity (Z_H) and temperature data inputs. Prior to HID analysis, ARMOR data were corrected for attenuation and processed to obtain specific differential phase (K_{DP}) through in-house implementation of the Bringi et al. [2001] methods. The Dolan et al. [2013] HID algorithm is included as part of the CSU Radar Tools python software package [Dolan et al. 2002]. To fascilitate their use with the python-based implementation of the algorithm, ARMOR data were imported and gridded with 1.0 km horizontal and 0.5 km vertical grid spacing utilizing the Python Advanced Radar Tools (Py-ART) package prior to HID analysis [Helmus et al. 2016]. In addition to qualitative analysis, gridded HID data were used to compute graupel volumes within the storm, derived from the number of grid pixels corresponding to either graupel category.

III. Results

During the analysis period from 0100 UTC to 0200 UTC, supercell lightning flash rates were observed between 1.5 fpm and 59.0 fpm, a time series of which is shown in Fig. 2. Three lightning jumps occurred during this period at 0130 UTC, 0136 UTC, and 0142 UTC, as well as one lightning dive at 0146 UTC. While these significant lightning flash rate trends constitute the focus of analysis, traditional bulk properties of the thunderstorm are first addressed.

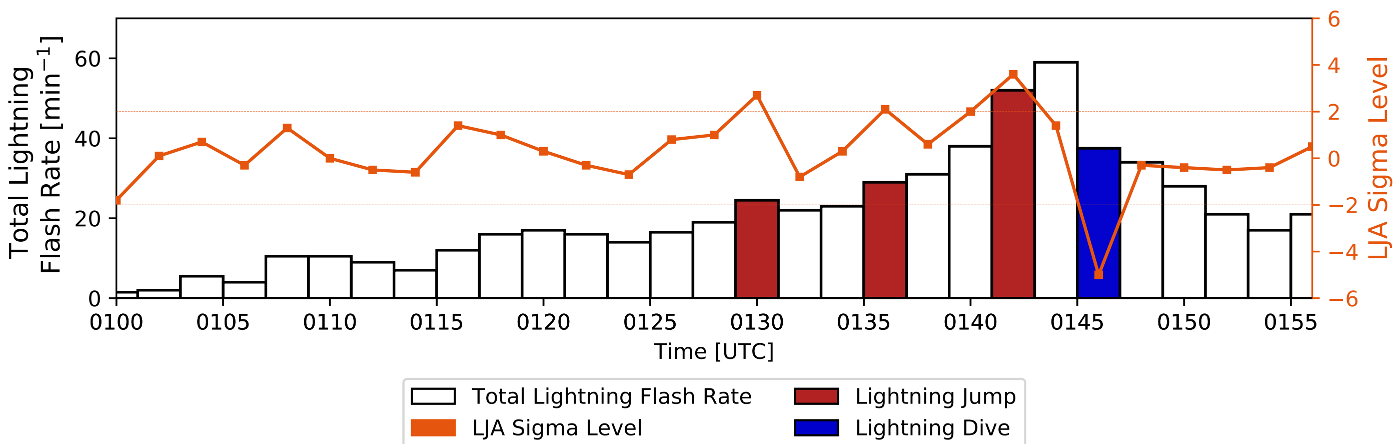

Fig. 2. Time series of flash rate and LJA information. Flash rate (black histogram) and s-level (orange line) are plotted against the left and right axes, respectively. Times at which a lightning jump occurred are marked in red and times at which a lightning dive occurred are marked in blue.

A. *Bulk Kinematic Properties*

Vertical wind data were evaluated during the analysis periods at time intervals corresponding to the ARMOR volume scan start times. Note that the quality of dual-Doppler analysis became markedly degraded beginning at 0136 UTC as the MAX radar signal was attenuated by heavy precipitation. After 0136 UTC, relative extrema and quality of vertical motion may be assessed, though data are not suitable for quantitative analysis.

To allow comparison of broad updraft properties with flash rates as accomplished in other studies, maximum updraft velocity and 10 m s^{-1} mixed-phase updraft volume were identified at each gridded plane above ground level (AGL), illustrated in Fig. 3. For reference, the mixed-phase region is defined between the heights of 0°C and -40°C, correponding to 3.9 km and 9.9 km for this storm environment. Additionally, the height of -10°C was located at 5.2 km.

The relative position and intensity of the updraft is of interest when considering the response of lightning flash properties to kinematics. Generally, the 10 m s^{-1} updraft volume remained at or below 36 km^3 until 0126 UTC, nearest to the time of the first lightning jump. At 0131 UTC, total 10 m s^{-1} updraft volume relaxed from a maximum of 102 km^3, mostly distributed between 5.5 km and 9.0 km, to a volume of 57 km^3, mostly distributed between 4.5 km and 6.0 km. Despite the general decline in magnitude, vertical extent, and altitude of the 10 m s^{-1} updraft volume, a second lightning jump occurred at 0136 UTC. Updraft volume characteristics are not available after 0136 UTC given the poor data quality. However, these observed trends between flash rate and updraft speed and 10 m s^{-1} updraft volume agree well with those quantified in previous work [e.g., Schultz et al. 2017].

B. *Spatial Behavior of Lightning and Microphysics with Respect to the Updraft*

The correspondence of temporal trends in flash rate, graupel volume, and vertical velocity have been discussed extensively in the lightning jump literature, though their spatial relationships are not frequently reported. To consider how graupel fields and lightning flashes relate in space to the updraft, as well as to each other, the locations of these properties were evaluated through time with respect to the three-dimensional location of the maximum vertical velocity of the updraft region.

For comparison of graupel regions with the location of the updraft, the median x-coordinate position and y-coordinate position were identified at each altitude at each radar analysis time. The median location point was evaluated against the location of the maximum updraft to determine a direction with respect to the updraft as well as the range of the graupel field from the maximum updraft. These results are shown in Fig. 4. Additionally, the positions of large values of FID and FED were considered. To determine regions of maximum FID

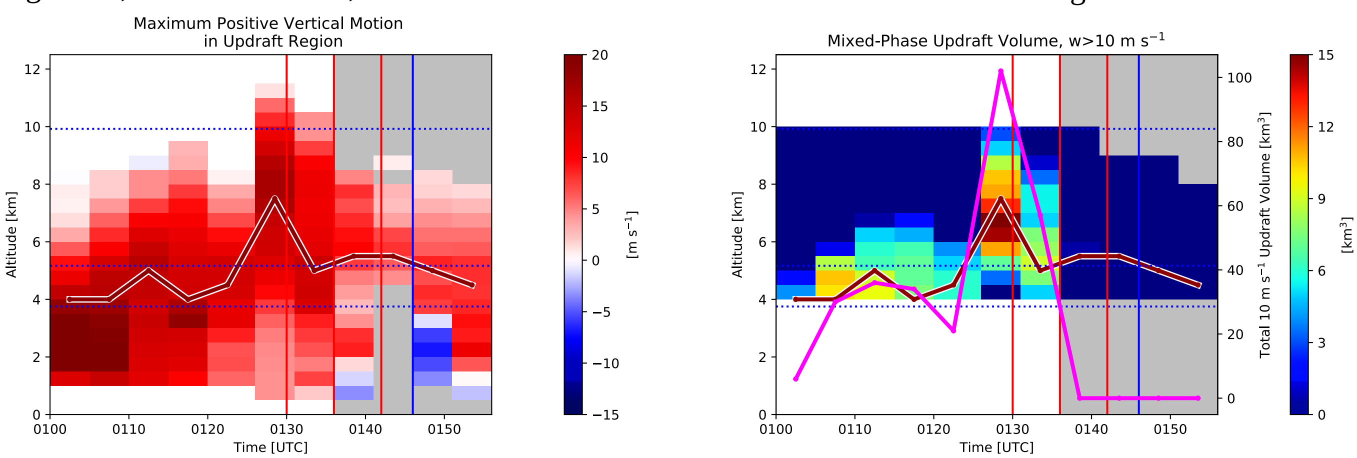

Fig. 3. Time-height plots of maximum vertical velocity within the main updraft region of the supercell (color-filled, left) and of 10 m s^{-1} updraft volume (color-filled, right). Times of poor dual-Doppler quality are shaded in gray. Within each panel, altitudes of 0°C, -10°C, and -40°C (horizontal dashed blue lines) and the altitude of the maximum vertical velocity within the updraft column at each time (dark red line, outlined in white) are also marked. Lightning jump (red) and lightning dive (blue) times are shown as vertical lines. Additionally, the total updraft volume is plotted in violet within the right panel along the right vertical axis.

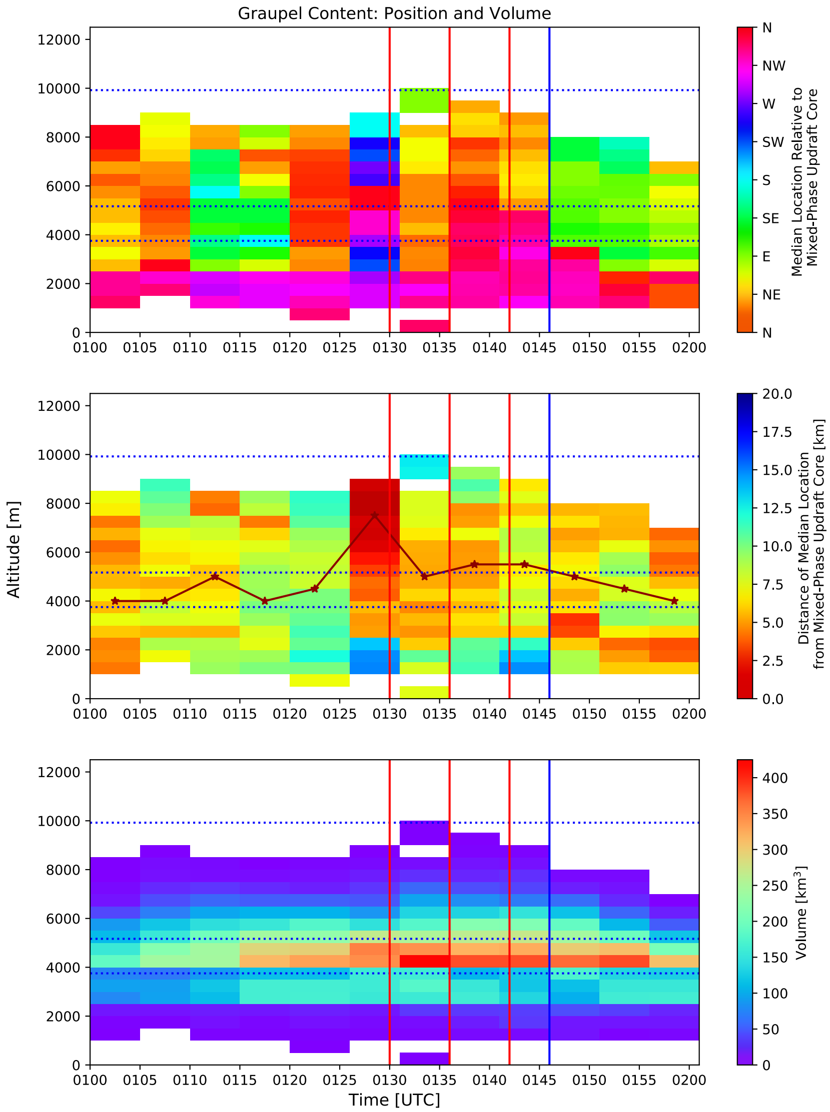

Fig. 4. Time series of the position (top) and range (middle) of the median graupel field location with respect to the maximum updraft, along with graupel volume within the storm (bottom) with height. The altitude of the maximum vertical velocity within the updraft column at each time (dark red line) is also included in the middle panel. Heights of 0°C, -10°C, and -40°C (horizontal dashed blue lines) and markers at the times of lightning jumps and dives (red and blue vertical lines) are shown in each panel.

and FED, the 90th percentile value of each property was calculated at each altitude level at each time. The median x-coordinate position and y-coordinate position of values greater than or equal to the 90th percentile values were evaluated against the location of the maximum updraft, as was done with the median graupel location. Results from analysis of the position of lightning properties are shown in Fig. 5.

While graupel volume increased steadily within the lower mixed-phase region of the storm, the first lightning jump at 0130 UTC occurred during an increase in graupel volume near the -10°C level and coincident with an increase in height in the maximum updraft from 4.5 km to 7.5 km. At this time, graupel distance from the maximum updraft position decreased substantially from over 7.5 km to less than 3.0 km through the mixed-phase region, with shortest distances coinciding with the height of the maximum updraft. Simultaneously, the ranges of large FID and FED values from the updraft decreased to less than 5.0 km and were comparable with graupel ranges from the updraft in the mixed-phase region. In contrast, the nearest large FID and FED values were slightly displaced above the altitude of the maximum updraft by approximately 2.0 km and more so above the altitudes of the greatest updraft volumes at this time (Fig. 3),

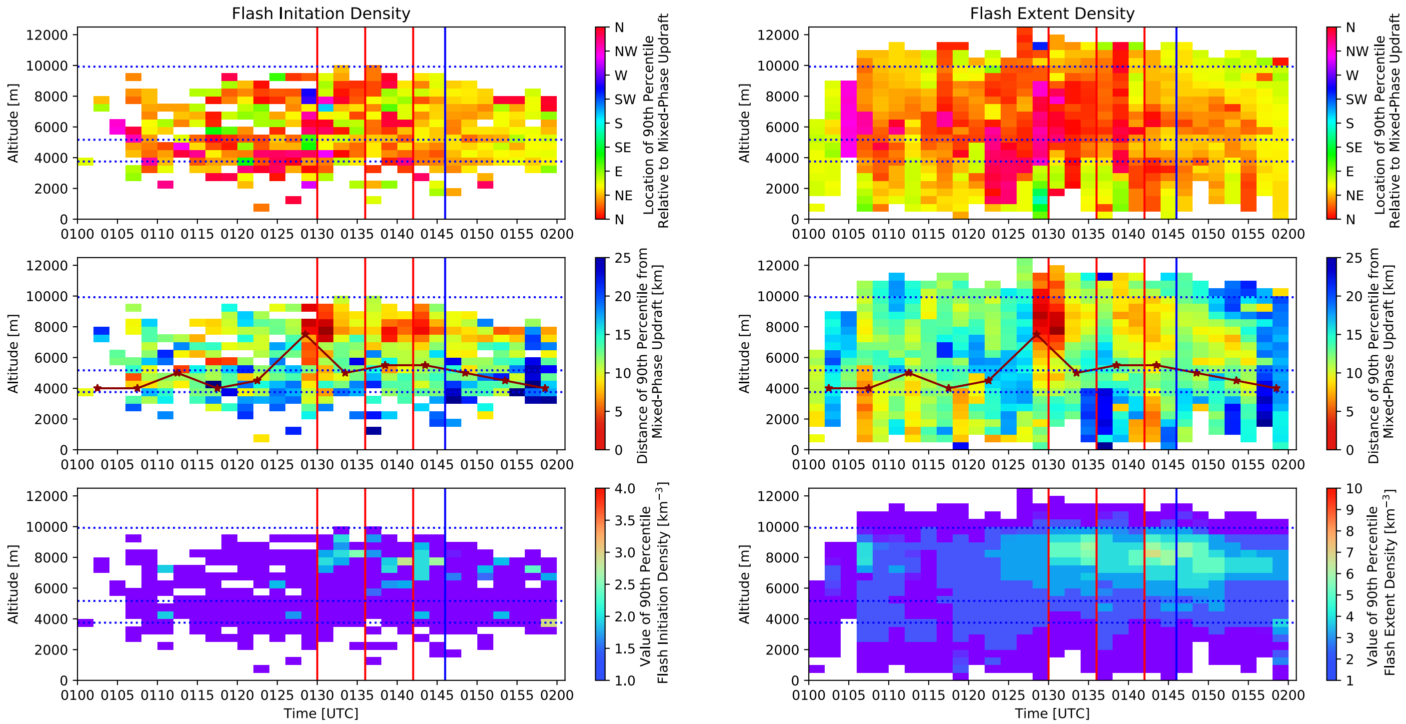

Fig. 5. Time series of the position (top) and range (middle) of the median significant flash initiation density (FID, left) and flash extent density (FED, right) locations with respect to the maximum updraft. Here, significant FID and FED were considered to be values greater than or equal to the 90th percentile value observed at each altitude and time (bottom). The altitude of the maximum vertical velocity within the updraft column at each time (dark red line) is included in the middle panels. Heights of 0°C, -10°C, and -40°C (horizontal dashed blue lines) and markers at the times of lightning jumps and dives (red and blue vertical lines) are shown in each panel.

consistent with observations made by Schultz et al. [2015, 2017]. With respect to relative position, it appears that graupel became more oriented to the west/southwest of the updraft, though this observation is likely an effect of the proximity of the graupel to the updraft versus a true change in relative directional location. Similar displacements were observed in FID in the regions of minimum range from the updraft, though to a lesser extent. Directional displacements and changes thereof were not as evident in FED.

At the time of the second lightning jump at 0136 UTC, the relatively small distances between the maximum updraft and graupel and lightning property fields had expanded from 1 km to 3 km in the mixed phase region to values of approximately 5 km to 7 km. Their relative positions also shifted to the north/northeast of the updraft. However, graupel volume increased in magnitude by approximately 50 km^3 per level and expanded with altitude within the mixed-phase region at this time. Maxima in the 90th percentile values of FID and FED were observed between 7.5 km and 9.5 km.

Spatial characteristics of lightning and graupel properties with respect to the updraft location at the time of the third lightning jump showed some similarities as well as differences compared with behavior observed during the previous two jumps. For instance, the relative distance between the graupel field and the updraft continued to increase, while mixed-phase graupel volume remained consistent. Maximum FID and FED values displayed a second period of relative maxima near the 7.5 km level, while their locations became closer to the location of the maximum updraft than observed during the previous jump at ranges of less than 7 km.

During the single lightning dive that occurred at 0146 UTC, the distance of graupel from the main updraft decreased and transitioned further to the east of the updraft. While a similar displacement was not discernible in the lightning FID and FED location data, the distance between substantial FID and FED and the main updraft increased to approximately 15 km throughout the mixed-phase levels. Consistent with a rapid decrease in lightning, 90th percentile FID values also decreased. However, increased 90th percentile FED values observed at the time of the third lightning jump persisted and extended through more of the lower mixed-phase region, though were located in decreasing proximity to the east/northeast of the updraft.

C. *Flash Properties During Periods of Substantial Flash Rate Trends*

Consideration of the spatial components of lightning flashes with respect to kinematics implied a degree of variability in flash properties between distinct lightning jumps. Flash initiation locations and flash sizes were more closely examined to further explore the characteristics of their variation.

Flash size and altitude of initiation of flashes within 2-min periods were examined for 10 min prior to the first lightning jump through 2 min after the lightning dive (Fig. 6). Though a small number of larger flashes (length ≥ 20 km) occurred near the -10°C altitude of the mixed-phase region sporadically during the analysis period, most flash lengths were typically smaller during lightning jump periods (length < 15 km), with the majority of small flashes occurring between 7 km and 9 km. The relative distributions of flash sizes greater than 10.0 km were similar for periods from 0120 UTC through 0140 UTC, including at the times of lightning jumps within that range. However, at 0142 UTC when the third jump occurred, the relative number of flashes ≥ 10 km decreased by approximately half of the percentage observed in earlier periods. The number of flashes during this period increased, consistent with the observation of a lightning jump. It is worth noting that while most of these were small flashes likely near to the updraft as suggested in Fig. 5, there were also a greater number of larger flashes observed between 6.0 km and 8.0 km. During the period of the lightning dive at 0146 UTC, while the majority of flashes were still ≤ 6 km in length, relatively more of these flashes were clustered at lower altitudes between 4.0 km and 6.0 km as opposed to the 7.0 km to 9.0 km range observed during the jumps. This vertical distribution persisted through 0148 UTC. Generally, between the time of the third jump at 0142 UTC and through the period after the dive at 0148 UTC, the number of flashes with lengths > 10 km also increased throughout the mixed-phase

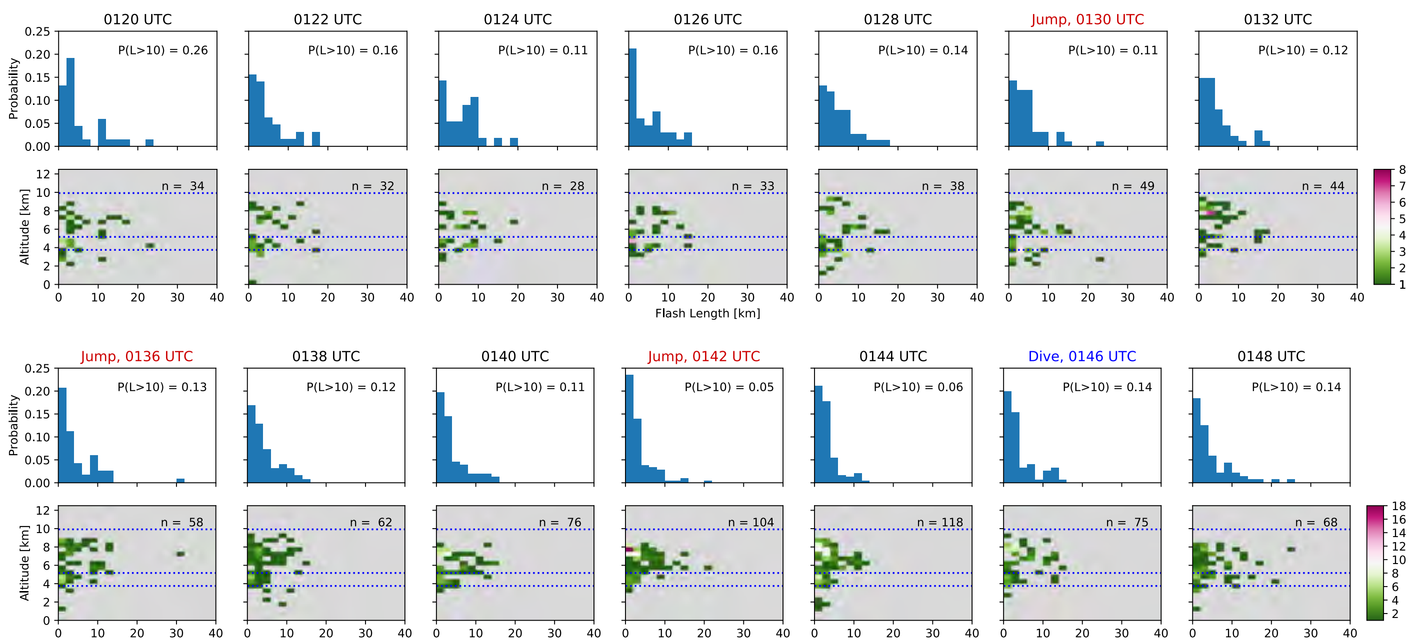

Fig. 6. Distributions of flash length within 2-min periods (top) and distributions of flash length with altitude within 2-min periods (bottom). The relative percentage of flashes with a length greater than 10 km are annotated in the top rows of each panel. The number of flashes within each 2-min bin are annotated in the bottom rows of each panel. The number of flashes of a given length that occurred at a given altitude are colored according to scales on the right, per row. Note that the scales corresponding to each row are different. The 2-min intervals corresponding to the times of the jumps (dive) are denoted by red (blue) text.

region.

It has been suggested that flash size and location respond to the coupled nature of the distribution of charge regions relative to a) microphysical constituents and b) kinematic texture associated with strong vertical motion [Bruning et al. 2007; Bruning and MacGorman 2013; Schultz et al. 2015]. Evaluation of lightning properties in the context of these convective components may facilitate understanding of relative roles in the nature of flash production with respect to flash rate trends.

Combining the spatial information of the hydrometeor fields and flash properties at the time of the first jump at 0130 UTC, Figs. 7a and 7b show numerous larger flashes at 5.5 km to 6.0 km at the periphery of the graupel region to the north of the updraft. Meanwhile, the majority of smaller flashes at 7.5 km to 8.0 km occurred in close proximity to the 10 m s^{-1} updraft volume, also along the periphery of the low-density graupel observed at 7.5 km. These depictions support information from Figs. 4 and 5 indicating that greater flash initiations were likely collocated with the primary graupel regions as evidenced by their similar close proximity to the updraft maximum location.

At the time of the second jump at 0136 UTC, Figs. 4 and 5 indicated that graupel and flash regions had shifted to the ENE of the maximum updraft and had also increased somewhat in range from the updraft. Figs. 7c and 7d show that the graupel region had expanded, particularly within the 5.0 km to 6.0 km levels of the mixed-phase region, while most lightning flashes occurred either along the northeastern periphery of the graupel near 5.0 km or further aloft near 8.0 km to 9.0 km. While the maximum updraft was located to the southwest of the storm, a new, secondary updraft region had begun to develop to the northeast between 7.5 km and 10 km. The weaker secondary updraft was evident at the 8.5 km level with a small region of 10 m s^{-1} updraft volume (Fig. 7d). Though more dispersed relative to the new updraft than flashes observed near the main updraft during the first lightning jump, flash initiation locations were closer to the new secondary updraft than the main updraft. The proximity of lightning initiation points to the secondary updraft as well as their spatial dispersion relative to the weaker vertical motion indicate that lightning was responding to the new updraft location and associated microphysics. After 0136 UTC, quantitative kinematic information is not available. However, similar observations from additional data may provide insight into the utility of the spatial information of lightning to inform about updraft growth processes as a complement to radar interpretation.

The third lightning jump occurred at 0142 UTC when quantitative updraft information was not available, though updraft location could still be loosely ascertained. Fig. 5 indicates that most lightning at the time of this jump was associated with the main updraft, where Fig. 7e and Fig. 7f suggest that this was the newly formed updraft seen in Fig. 7d. At the time of the third jump, a large number of small flashes were observed near the position of the updraft, in close proximity with the low density graupel region observed in Fig. 7f. As suggested by the information in Fig. 6, a large number of larger flashes were also observed along a line from NNW of the main updraft to E of the main updraft. These larger flashes occur between 5.5 km and 7.5 km, and appear to be associated with a relatively expansive region of graupel near 6.0 km.

Flash properties of the lightning dive at 0146 UTC and flash data from the subsequent 2-min period at 0148 UTC are shown in Figs. 8a and 8b. During this period, a relatively large number of small flashes was observed distributed throughout the storm, as indicated by the distance from the updraft seen in Fig. 5 and the relative distribution of flash size observed in Fig. 6. Generally, flashes appear to have responded less to the updraft, though in absence of quantitative kinematic information, it is not possible to ascertain any measure of the strength of the updraft at this time. However, qualitative flash properties indicate that the updraft was not supporting or influencing flash behavior during this period as observed during the lightning jumps. It is suggested that the lightning dive observed in this instance was a response to the decreased capability of the updraft to support mixed-phase updraft growth and particle-

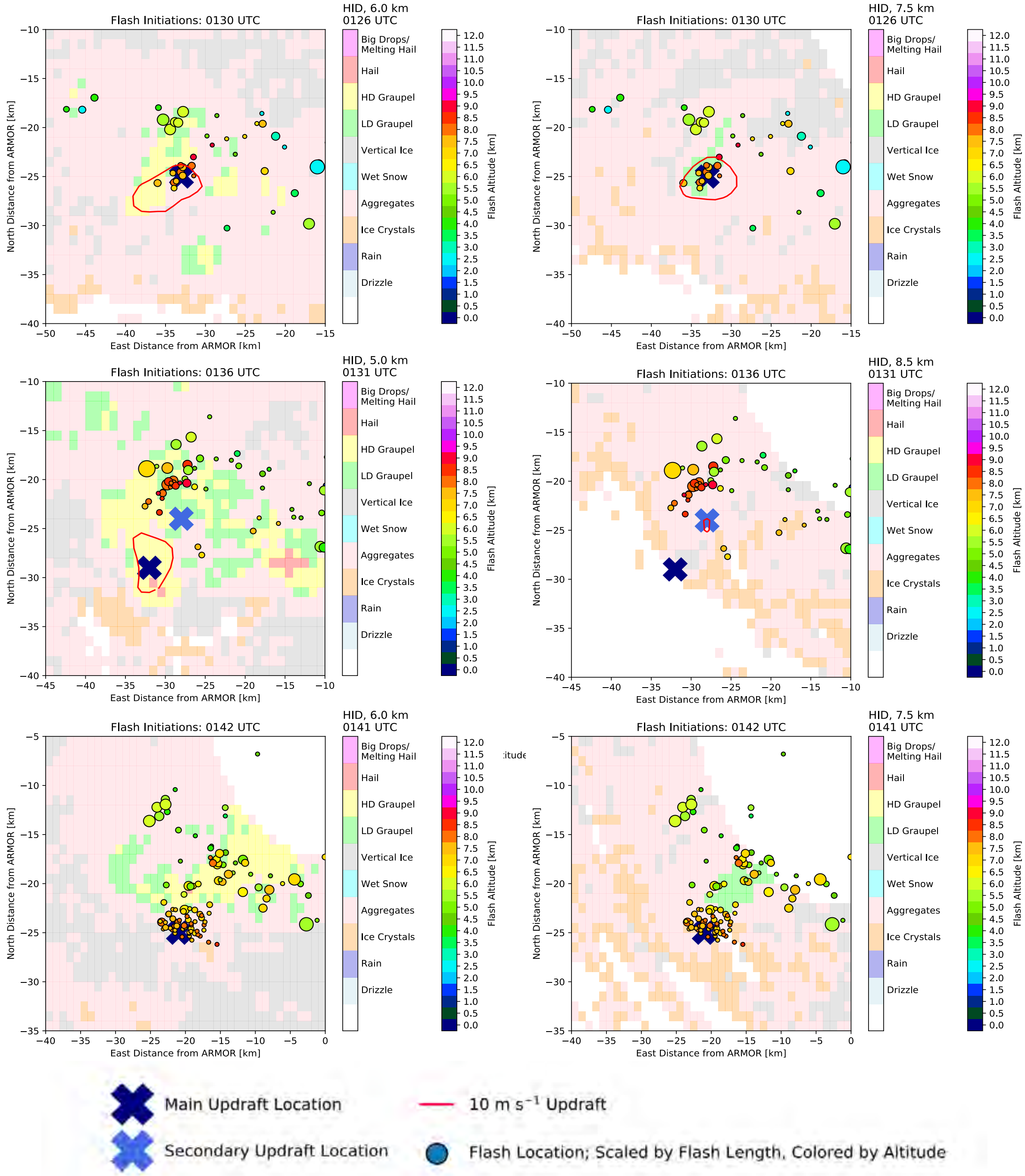

Fig. 7. Plots of lightning flash initiation locations in two minute intervals corresponding to the lightning jumps at 0130 UTC (a,b), 0136 UTC (c,d), and 0142 UTC (e,f). Flash points are marked as circles, colored by altitude of initiation and sized according to relative length. Flashes are plotted over planar images of HID at corresponding ARMOR volume times at various altitudes, marked above the left-most color bar in each panel. The 10 m s^{-1} updraft contour is plotted (red line) along with the location of the main updraft (dark blue cross). When a secondary updraft is present (c,d), its location marked (light blue cross) in addition to that of the main updraft.

scale charge separation through its influence on rebounding collisions. This behavior was coincident with mesocyclogenesis inferred from Doppler velocity data, where the reported tornado was associated with the new mesocyclone [Vacek 2017]. Further, flashes appear to have transitioned to lower altitudes during and following the time of the lightning dive. Simultaneously, graupel volume trends indicate that graupel may have been descending within the storm, particularly as values between 4.0 km and 6.5 km decreased while values between 3.5 km and 4.0 km increased.

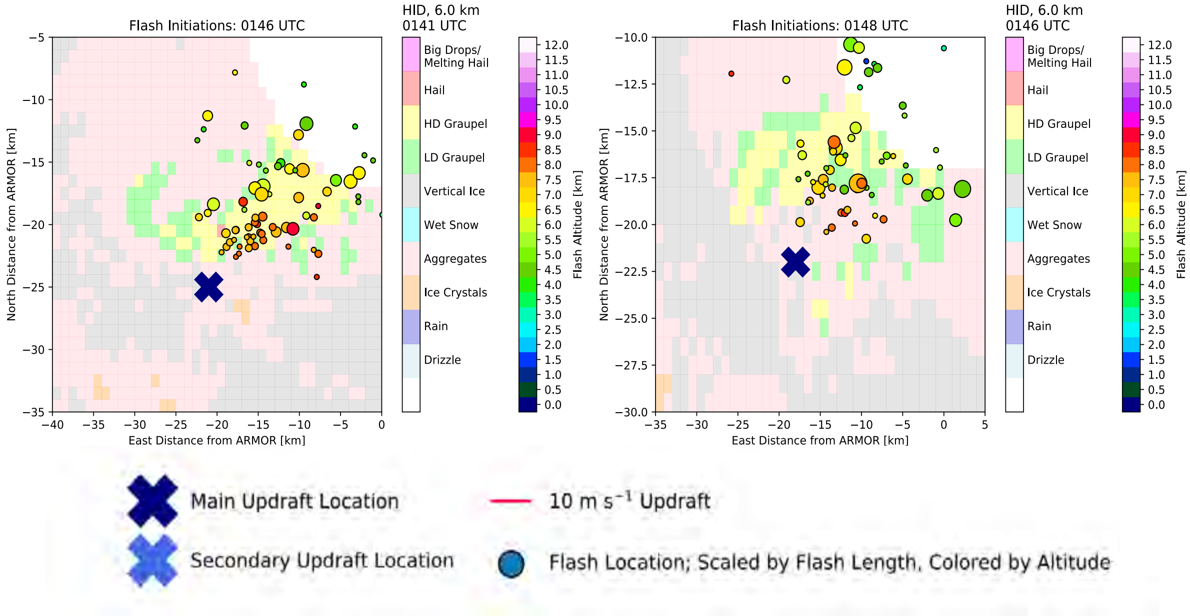

Fig. 8: As described in Fig. 7 for the lightning dive period at 0146 UTC (a) and the subsequent 2-min period at 0148 UTC (b).

IV. Summary and Direction of Continuing Work

This study considered details within bulk trends in lightning, kinematic, and microphysical thunderstorm properties observed in a supercell thunderstorm as a preliminary evaluation of the complexities between lightning and thunderstorm microphysics and kinematic relationships.

Prior to addressing flash properties and spatial relationships with microphysical and kinematic fields, it was first noted that broad trends between lightning flash rates and updraft properties were consistent with those documented in the literature. Upon examining the spatial nature of the evolution of lightning properties and microphysics with respect to the updraft, variability in properties of lightning flashes associated with lightning jumps emerged. Specifically, it was observed that while regions in which many flashes formed and propagated corresponded closely in space with mixed-phase graupel regions, their locations each tended to vary with respect to the location of the main updraft at the times of different lightning jumps. Examing flash properties during each period in more detail, variations in flash size with altitude at the times of different jumps were apparent, consistent with observed spatial changes in FED in particular.

Placing these properties in the context of microphysics, it was observed that dominant sizes and preferential altitudes of flash initiation were associated with kinematics as well as the spatial distribution of graupel regions. Moreover, dominant flash sizes and apparent preferential altitudes of flash initiation during lightning jumps appeared to respond to a complex combination of the presence of graupel near regions of vertical velocity. As a specific example, lightning that occurred during the second observed lightning jump at 0136 UTC was spatially associated with a region of developing vertical velocity aloft and nearby graupel rather than with graupel fields in the vicinity of the stronger, broader updraft.

Lightning dives have been observed for some time, particularly with respect to tornadogenesis [e.g., Steiger et al. 2007], though their physical nature has only recently been addressed [Vacek 2017]. Characterization of flash properties associated with lightning dives is therefore limited. However, these analyses indicate that a lightning dive is not only characterized differently from lightning jumps in terms of the numbers of flashes that occur, but may also differ with respect to how flashes are distributed within the storm. Specifically, while the distribution of flash size was similar during the dive as observed at other periods during the storm, smaller flashes were not clustered near the main updraft but rather were more distributed throughout graupel regions that extended to lower altitudes.

Additional analyses are necessary as part of future work to characterize the variability of lightning during significant trends in flash behavior. Goals of ongoing work are to clarify the respective roles of microphysics and kinematics in the generation of a lightning jump, thereby refining understanding of how these lightning trends relate to thunderstom intensity. Additionally, better understanding of the physical basis of lightning dives requires further observation to understand the information they may provide concerning thunderstorm processes.

ACKNOWLEDGMENT

We gratefully acknowledge Austin Vacek for providing dual-Doppler analysis data as an essential component of this research.

REFERENCES

Bruning, E. C. (2013), Streamed clustering of lightning mapping data in Python using sklearn, presented at 12th Python in Science Conference (SciPy), vol. 2, Austin, Texas, United States.

Bruning, E. C., and D. R. MacGorman, (2013), Theory and observations of controls on lightning flash size spectra. J. Atmos. Sci., 70, 4012–4029, doi:10.1175/JAS-D-12-0289.1. http://journals.ametsoc.org/doi/abs/10.1175/JAS-D-12-0289.1.

Bruning, E. C., W. D. Rust, T. J. Schuur, D. R. MacGorman, P. R. Krehbiel, and W. Rison, (2007), Electrical and polarimetric radar observations of a multicell storm in TELEX. Mon. Weather Rev., 135, 2525–2544, doi:10.1175/MWR3421.1.

Calhoun, K. M., D. R. MacGorman, C. L. Ziegler, and M. I. Biggerstaff, (2013), Evolution of lightning activity and storm charge relative to dual-Doppler analysis of a high-precipitation supercell storm. Mon. Weather Rev., 141, 2199–2223, doi:10.1175/MWR-D-12-00258.1.

Calhoun, K. M., E. R. Mansell, D. R. MacGorman, and D. C. Dowell, (2014), Numerical simulations of lightning and storm charge of the 29-30 May 2004 Geary, Oklahoma supercell thunderstorm using EnKF mobile radar data assimilation. Mon. Weather Rev., 142, 140709125303002, doi:10.1175/MWR-D-13-00403.1.

Carey, L. D., and S. A. Rutledge, (1996), A multiparameter radar case study of the microphysical and kinematic evolution of a lightning producing storm. Meteorol. Atmos. Phys., 59, 33–64, doi:10.1007/BF01032000.

Carey, L. D., and S. A. Rutledge, (2000), The relationship between precipitation and lightning in tropical island convection: A C-band polarimetric radar study. Mon. Weather Rev., 128, 2687–2710, doi:10.1175/1520-0493(2000)128<2687:TRBPAL>2.0.CO;2.

Darden, C. B., D. J. Nadler, B. C. Carcione, R. J. Blakeslee, G. T. Stano, and D. E. Buechler, (2010), Utilizing total lightning information to diagnose convective trends. Bull. Am. Meteorol. Soc., 91, 167–175, doi:10.1175/2009BAMS2808.1.

Deierling, W., and W. A. Petersen, (2008), Total lightning activity as an indicator of updraft characteristics. J. Geophys. Res., 113, D16210, doi:10.1029/2007JD009598.

Deierling, W., W. A. Petersen, J. Latham, S. Ellis, and H. J. Christian, (2008), The relationship between lightning activity and ice fluxes in thunderstorms. J. Geophys. Res., 113, D15210, doi:10.1029/ 2007JD009700.

Dolan, B., B. Fuchs, K. Wiens, R. Cifelli, L. Carey, T. Lang and Coauthors, (2002), CSU Radar Tools, accessed 2016. [Available online at https://github.com/CSURadarMet/CSU_RadarTools.]

Dolan, B., S. A. Rutledge, S. Lim, V. Chandrasekar, and M. Thurai, (2013), A robust C-band hydrometeor identification algorithm and application to a long-term polarimetric radar dataset. J. Appl. Meteorol. Climatol., 52, 2162–2186, doi:10.1175/JAMC-D-12-0275.1.

Fuchs, B. R., E. C. Bruning, S. A. Rutledge, L. D. Carey, P. R. Krehbiel, and W. Rison, (2016), Climatological analyses of LMA data with an open-source lightning flash-clustering algorithm. J. Geophys. Res. Atmos., 121, 8625–8648, doi:10.1002/2015JD024663.Received.

Fuchs, B. R., and Coauthors, (2015), Environmental controls on storm intensity and charge structure in multiple regions of the continental United States. J. Geophys. Res. Atmos., 120, 6575–6596, doi:10.1002/2015JD023271.

Gatlin, P. N., and S. J. Goodman, (2010): A total lightning trending algorithm to identify severe thunderstorms. J. Atmos. Ocean. Technol., 27 (1), 3–22, doi:10.1175/2009JTECHA1286.1.

Goodman, S. J., and Coauthors, (2005), The North Alabama Lightning Mapping Array: Recent severe storm observations and future prospects. Atmos. Res., 76, 423-437.

Heistermann, M., and Coauthors, (2014), The emergence of open source software for the weather radar community. Bull. Amer. Meteor. Soc., 96, 117–128, doi:https://doi.org/10.1175/BAMS-D-13-00240.1.

Helmus, J. J. and Collis, S. M., (2016), The Python ARM Radar Toolkit (Py-ART), a library for working with weather radar data in the Python programming language. J. of Open Research Software. 4 (1), p.e25. doi:http://doi.org/10.5334/jors.119.

Hookings, G. A., (1965), Precipitation-maintained downdrafts. J. Appl. Meteorol., 4 , 190–195.

Knupp, K. R., (1987), Downdrafts within High Plains cumulonimbi. Part I: General kinematic structure. J. Atmos. Sci., 44, 987–1008, doi:10.1175/15200469(1988)045<3965:DWHPCP>2.0.CO;2.

Knupp, K. R., (1988), Downdrafts within High Plains cumulonimbi. Part II: Dynamics and thermodynamics. J. Atmos. Sci., 45, 3965–3982, doi:10.1175/1520-0469(1988)045<3965:DWHPCP>2.0.CO;2.

Knupp, K. R., and Coauthors, (2014), Meteorological Overview of the Devastating 27 April 2011 Tornado Outbreak. Bull. Amer. Meteor. Soc., 95, 1041–1062, doi: 10.1175/BAMS-D-11-00229.1.

Koshak, W. J., and Coauthors, (2004), North Alabama Lightning Map- ping Array (LMA): VHF source retrieval algorithm and error analyses. J. Atmos. Ocean. Technol., 21 (4), 543–558, doi:10.1175/1520-0426(2004)021⟨ 0543:NALMAL⟩ 2.0.CO;2.

Lakshmanan, V., T. Smith, G. Stumpf, and K. Hondl, (2007), The Warning Decision Support System–Integrated Information. Weather Forecast., 22, 596–612, doi:10.1175/WAF1009.1.

Lang, T. J., and S. A. Rutledge, (2002), Relationships between convective storm kinematics, precipitation, and lightning. Mon. Wea. Rev., 130 (10), 2492–2506, doi:10.1175/15200493(2002)130⟨ 2492:RBCSKP⟩ 2.0.CO;2.

Lemon, L. R., and C. A. Doswell, (1979), Severe Thunderstorm Evolution and Mesocyclone Structure as Related to Tornadogenesis. Mon. Wea. Rev., 107 (9), 1184–1197..

McCaul, E. W., J. Bailey, J. Hall, S. J. Goodman, R. Blakeslee, and D. E. Buechler, (2005), A flash clustering algorithm for North Alabama Lightning Mapping Array data. Conf. on Meteoro- logical Applications of Lightning Data, San Diego, CA, Amer. Meteor. Soc., 5.3, http://ams.confex.com/ams/Annual2005/techprogram/paper_84373.htm.

McCaul, E. W., S. J. Goodman, K. M. LaCasse, and D. J. Cecil, (2009), Fore-casting lightning threat using cloud-resolving model simulations. Wea. Forecasting, 24, 709–729, https://doi.org/10.1175/2008WAF2222152.1.

Miller, L. J., and S. M. Fredrick, (1998), CEDRIC: Custom Editing and Display of Reduced Information in Cartesian Space. Manual, Mesoscale and Microscale Meteorology Division, National Center for Atmospheric Research, 130 pp.

Mohr, C. G., L. J. Miller, R. L. Vaughn, and H. W. Frank (1986), On the merger of mesoscale datasets into a common Cartesian format for efficient and systematic analysis, J. Atmos. Oceanic. Technol., 3(1), 143–161.

Oye, D., and M. Case, (1995), REORDER: A program for gridding radar data installation and use manual for the Unix version. National Center for Atmospheric Research, 44 pp. [Available online at http://www.eol.ucar.edu/content/reorder-reference-manual.]

Naylor, J., M. a. Askelson, and M. S. Gilmore, (2012), Influence of low-level thermodynamic structure on the downdraft properties of simulated supercells. Mon. Weather Rev., 140, 2575–2589, doi:10.1175/MWR-D-11-00200.1.

NASA, (2001), North Alabama Lightning Mapping Array data. NASA Global Hydrology Resource Center, Huntsville, AL, accessed 2016, https://lightning.nsstc.nasa.gov/lma/nalma/data/.

Reynolds, S. E., M. Brook, and M. F. Gourley (1957), Thunderstorm charge separation, J. Meteor., 14, 426–436.

Rison, W., R. J. Thomas, P. R. Krehbiel, T. Hamlin, and J. Harlin, (1999), A GPS-based three-dimensional lightning mapping system: Initial observations in central New Mexico. Geophys. Res. Lett., 26, 3573–3576, https://doi.org/10.1029/1999GL010856.

Schultz, C. J., W. A. Petersen, and L. D. Carey, (2009), Preliminary development and evaluation of lightning jump algorithms for the real-time detection of severe weather. J. Appl. Meteor. Climatol., 48, 2543–2563, doi:10.1175/2009JAMC2237.1.

Schultz, C. J., W. A. Petersen, and L. D. Carey, (2011), Lightning and severe weather: A comparison between total and cloud-to-ground lightning trends. Wea. Forecasting, 26, 744–755, doi:10.1175/WAF-D-10-05026.1.

Schultz, C. J. and Coauthors, (2012), Dual polarization tornadic debris signatures Part I: Examples and utility in an operational setting. Electronic J. Operational Meteor., 13, 120-137.

Schultz, C. J., W. A. Petersen, and L. D. Carey, and R. J. Blakeslee, (2015), Insight into the kinematic and microphysical processes that control lightning jumps. Wea. Forecasting, 30, 1591–1621, doi:10.1175/WAF-D-14-00147.1.

Schultz, C. J., W. A. Petersen, and L. D. Carey, and R. J. Blakeslee, (2017), Kinematic and microphysical significance of lightning jumps versus nonjump increases in total flash rate. Wea. Forecasting, 32, 275–288, doi:10.1175/WAF-D-15-0175.1.

Srivastava, R. C., (1985), A simple model of evaporatively driven downdraft: Application to microburst downdraft. J. Atmos. Sci., 42, 1004–1023, doi:10.1175/1520-0469(1985)042<1004:ASMOED>2.0.CO;2.

Srivastava, R. C., (1987), A model of intense downdrafts driven by the melting and evaporation of precipitation. J. Atmos. Sci., 44, 1752–1774, doi:10.1175/1520-0469(1987)044<1752:AMOIDD>2.0.CO;2.

Stough, S. M., L. D. Carey, C. J. Schultz, and P. M. Bitzer, (2017), Investigating the Relationship between Lightning and Mesocyclonic Rotation in Supercell Thunderstorms. Weather Forecast., 32, 2237–2259, doi:10.1175/WAF-D-17-0025.1.

Takahashi, T., (1978), Riming electrification as a charge generation mechanism in thunderstorms. J. Atmos. Sci., 35, 1536–1548, doi:10.1175/1520-0469(1978)035<1536:REAACG>2.0.CO;2.

Thomas, R. J., P. R. Krehbiel, W. Rison, S. J. Hunyady, W. P. Winn, T. Hamlin, and J. Harlin, (2004), Accuracy of the lightning mapping array. J. Geophys. Res. D Atmos., 109, 1–34, doi:10.1029/2004JD004549.

Tong, H., V. Chandrasekar, K. R. Knupp, and J. Stalker, (1998), Multiparameter radar observations of time evolution of convective storms: Evaluation of water budgets and latent heating rates. J. Atmos. Ocean. Technol., 15, 1097–1109, doi:10.1175/1520-0426(1998)015<1097:MROOTE>2.0.CO;2.

Vacek, A. (2017), Identifying physical processes in supercells for nowcasting severe weather potential, M.S. thesis, Univ. of Ala. in Huntsville, Huntsville.

Vonnegut, B., 1996: Importance of evaporative cooling in the formation of thundercloud downdrafts. J. Appl. Meteorol., 35, 1378.

Williams, E., and Coauthors, (1999), The behavior of total lightning activity in severe Florida thunderstorms. Atmos. Res., 51, 245–265, doi:10.1016/S0169-8095(99)00011-3.